Multispacecraft Observations and Modeling of the June 22/23, 2015 Geomagnetic Storm

P. H. Reiff[1], A. G. Daou[1], S. Y. Sazykin[1], R. Nakamura[2], M. R. Hairston[3], V. Coffey[4], M. O. Chandler[4], B. Anderson[5], C. T. Russell[6], D. Welling[7], S. A. Fuselier[8,9] and K. J. Genestreti[9,8]

[1]Rice Space Institute, Rice University, Houston, TX.
[2]OEAW, Vienna, Austria.
[3]Center for Space Sciences, University of Texas at Dallas, Richardson, TX.
[4]Marshall Space Flight Center, Huntsville, AL.
[5]APL, Johns Hopkins University, Laurel, MD.
[6]IGPP, University of California at Los Angeles, Los Angeles, CA.
[7]University of Michigan, Ann Arbor, MI.
[8]Southwest Research Institute, San Antonio, TX.
[9]University of Texas at San Antonio, San Antonio, TX.

Corresponding Author: Patricia Reiff (reiff@rice.edu)

Key Points:

- MHD models can reproduce well the dipolarizations seen at MMS and VAP. Space weather forecasting can predict Kp variations within 0.5 step.
- Beams of O^+ flowing downstream appear to cross the separatrix and become a second energized population of the tail plasma sheet.
- MHD models successfully reproduced the polar cap convection patterns and cross-polar cap potential drops for a range of IMF conditions.

This is the author manuscript accepted for publication and has undergone full peer review but has not been through the copyediting, typesetting, pagination and proofreading process, which may lead to differences between this version and the Version of Record. Please cite this article as doi: 10.1002/2016GL069154

Abstract

The magnetic storm of June 22-23, 2015 was one of the largest in the current solar cycle. We present in situ observations from the Magnetospheric Multiscale Mission (MMS) and the Van Allen Probes (VAP) in the magnetotail, field-aligned currents from AMPERE, and ionospheric flow data from DMSP. Our real-time space weather alert system sent out a "red alert", correctly predicting Kp indices greater than 8. We show strong outflow of ionospheric Oxygen, dipolarizations in the MMS magnetometer data, and dropouts in the particle fluxes seen by the MMS FPI instrument suite. At ionospheric altitudes, the AMPERE data show highly variable currents exceeding 20 MA. We present numerical simulations with the BATS-R-US global magnetohydrodynamic (MHD) model linked with the Rice Convection Model (RCM). The model predicted the magnitude of the dipolarizations, and varying polar cap convection patterns, which were confirmed by DMSP measurements.

1 Introduction

On June 22, one moderate and one giant coronal mass ejection (CME) passed the ACE spacecraft at 04:51 and 17:58 UT respectively. The larger shock was observed by the MAG instrument [*Smith et al.*, 1998] as a jump in the IMF from about 10 to over 40 nT and by the SWEPAM instrument [*McComas et al.*, 1998] as a jump in solar wind density from 20 to over 45 particles/cm^3, with a corresponding increase in pressure to over 50 nPa. When propagated to the bowshock, it was forecast to impact at about 18:36 UT after a smaller shock at about 05:40 UT (Figure 1A). Coupled with a strong southward IMF (Figure 1D), the Boyle Index reached nearly 500 kV, prompting our forecast system [*http://mms.rice.edu/realtime/forecast.html*] to send out a "yellow alert" at 06:04 and a "red alert" at 18:34, even before the CME impacted the bow shock. The y-component of the IMF was very strong, with the IMF clock angle (Figure 1E), rotating anticlockwise then clockwise nearly 360 degrees. The neural network forecaster [*Bala and Reiff*, 2012] predicted Kp of over 8 and the Kp forecast status went to "red" at 19:02.

The magnetospheric flotilla of spacecraft included MMS, VAP, Themis, and Cluster in the magnetosphere, plus AMPERE, DMSP, and ISS at low altitudes. This paper will concentrate on the large-scale features of the activity. It will include selected MMS, VAP, AMPERE and DMSP results and compare to the BATS-R-US model simulations. Other papers in this issue (e.g. *Nakamura et al*; *Baker et al.*) will focus on other aspects of this event.

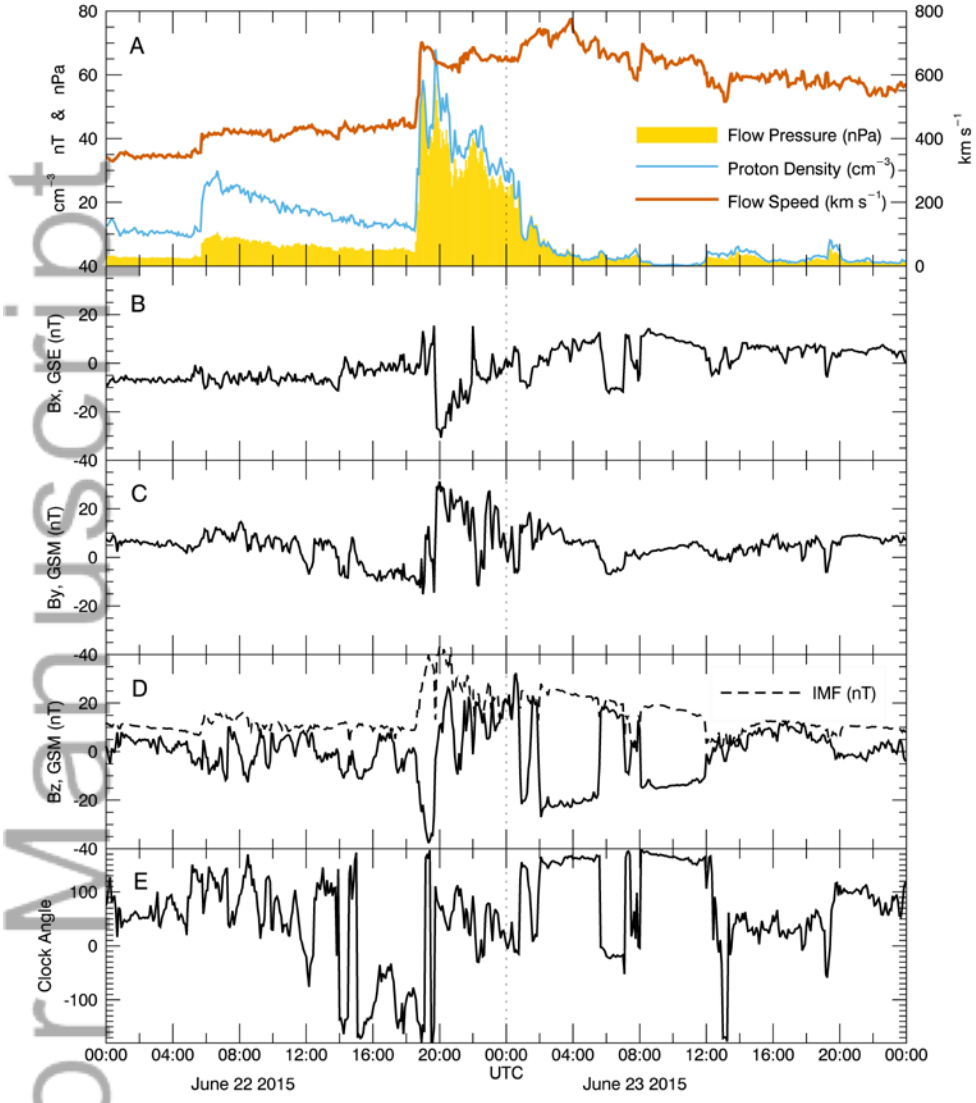

Figure 1. Interplanetary conditions during the event. A: solar wind density, velocity, and flow pressure; B, C, D: IMF Bx, By, Bz (and |B| shown dashed) components (GSM); E: IMF clock angle (0 = +Bz; 90 = + By direction). The values are plotted from OMNI data, propagated to the bow shock.

2 Space Weather Forecasting

The Rice University space forecast system *[http://mms.rice.edu/realtime/forecast.html]* predicts the Kp, AE, and Dst indices for one and three hours ahead of real time, at a cadence of 15 m. The

prediction is based on a neural network forecast that uses one or more base functions and look-back data of up to 24 hours. Yellow alerts are sent out if the forecast Kp is greater than 4, and red alerts if the forecast Kp is 6 or greater [*Bala and Reiff*, 2012]. Statistically, the accuracy of the predicted Kp is approximately one unit. Three base formulae are used in the forecast: the Boyle Index (marked as BI), the Boyle Index with a ram pressure term (RAM), and the Newell function (Newell) [*Bala and Reiff*, 2014]. All have similar prediction efficiencies, and the three predictions generally span the actual measured quantities. For this event, all three formulae gave similar predictions, with the AE index least well predicted (r = 0.61 to 0.72), whereas Kp and Dst were successful with r = 0.79 to 0.91 (Figure 2).

A comment on timing of "predictions" is in order. The forecast algorithm was trained on one-hour averages of AE, Dst, and Kp*, with the Kp* values being an overselection of Kp (because it is intrinsically a 3-hour average). The algorithm predicts the one-hour AE, Dst and Kp* values for the hour following, based on the solar wind data of the previous hour. The calculation is done at the top of the hour after the realtime solar wind data are received, and a forecast typically posted at 6 minutes past the hour for the hour of the forecast (e.g. 18:06 for the hour 18-19). In this case, because the shock hit at the very end of hour 17, the AE predictions for hour 18-19 were not as high as the provisional AE turned out to be (Figure 2C), because the forecast only included two minutes of post-shock data, and because the high solar wind speed meant that the shock arrived at earth well before the end of hour 18. The forecast 3-hour Kp, based on three-hour averages of the one-hour predictions (Figure 2A), does show a very good fit (r = .88 to .91, implying an accuracy of prediction from 0.36 to 0.47 step in Kp).

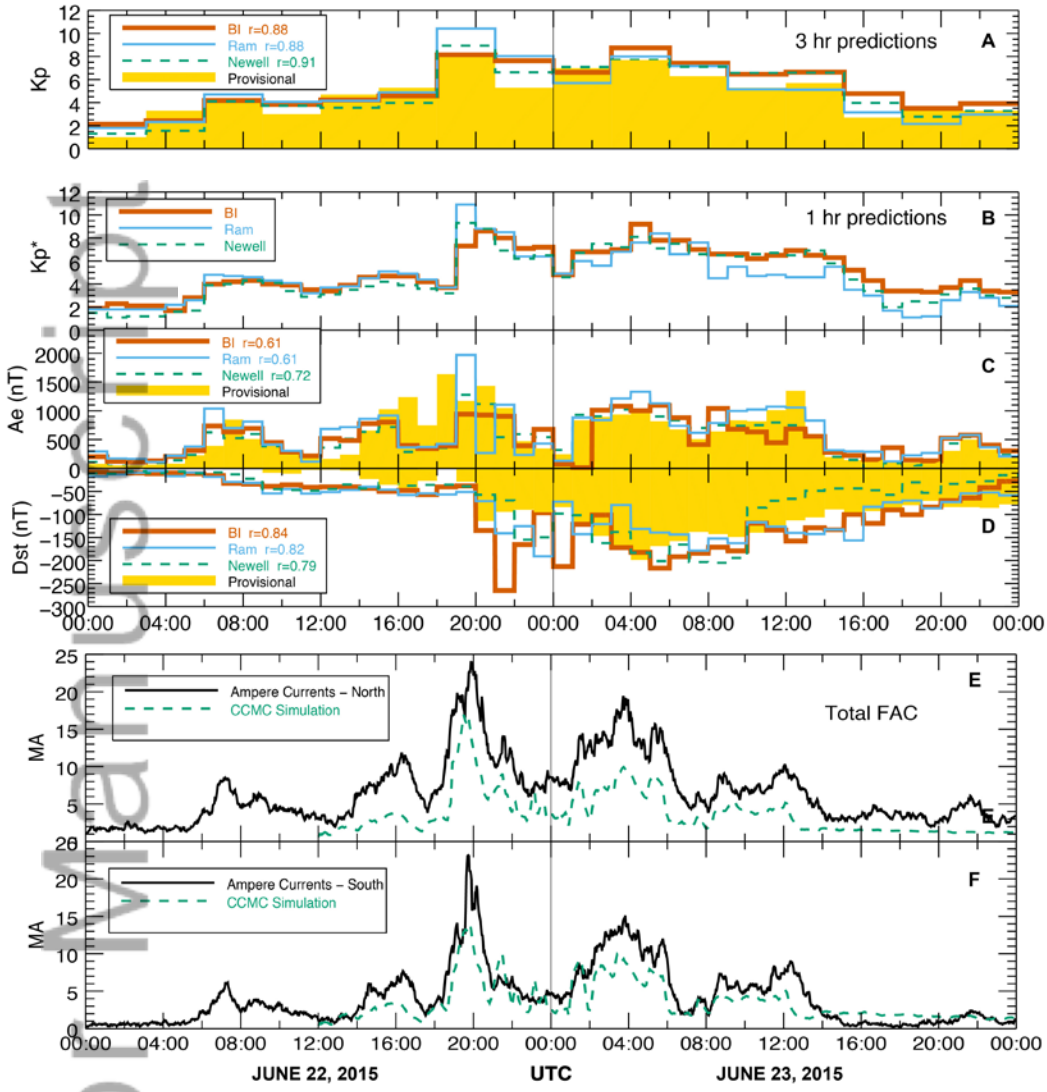

Figure 2. Comparison of predicted and modeled values compared to data. A shows the predicted 3-hour Kp index for June 22-23, 2015, compared to the provisional Kp, with a 90% correlation coefficient. Predicted (histograms) and observed provisional (yellow) Kp* (panel B), AE (panel C), and Dst (panel D) indices. All three base functions: BI (thick line), Ram (thin line) and Newell (dashed) performed well, some slightly better than others. Modeled integrated field aligned currents (dashed) versus those calculated from AMPERE measurements for the Northern (panel E) and Southern (panel F) hemispheres.

3 Magnetotail Observations

Since the MMS spacecraft suite [*Burch et al., 2015*] was in the "commissioning" phase of its mission, not all of the instruments were fully operational. All of the magnetometers [*Russell et*

al., 2015] and many of the particle detectors were making measurements and saw the dynamic response of the magnetosphere. The Fast Plasma Instrument (FPI) onboard MMS2 [*Pollock et al.*, 2015] saw a number of excursions between the plasma sheet and the lobe, shown in Figure 3 as particle flux dropouts at about 3:20-3:30 and 5:11-05:40 UT (Panels C and D). Clearly visible in the lobe are antisunward flowing ions, at a few hundred eV (Panels B and C). The Hot Plasma Composition Analyzer (HPCA) onboard MMS1 [*Young et al.*, 2015] identified these beams as O^+ (Panel B) presumably from auroral outflow [*Lu et al., 1992*] or possibly from the dayside cusp [*Liao et al.*, 2010] though cusp ions will more likely reach the neutral sheet farther downtail [*Liao et al.*, 2012]. The HPCA instrument, because of a new AC sweep field, can reduce background H^+ fluxes by nearly two orders of magnitude, making the determination of the heavy ion species much more reliable. This cool lobe ion beam appears to be accelerated and heated as it crosses into the plasmasheet. In Figure 3, Panels E- G, we show sample total-ion particle distributions from FPI MMS2 as the spacecraft exits the plasmasheet into the lobe around 05:10:30. In the lobe around 05:11:19 (panel G), we see two separated cold ion beams: one with a parallel velocity of around 50 km/s and another with a parallel velocity of ~200 km/s. The right image of that pair shows that those beams are also convecting at about the same **ExB** speed (v_{perp1}) as the parallel speeds, with no drift in the other direction (v_{perp2}) perpendicular to B. From the HPCA data (Panels A and B), it is clear that the less energetic ions are H^+ and the ones with apparently higher velocity are just O^+ ions with the same parallel and perpendicular velocity as the H^+ ions. This is confirmed by the HPCA particle distribution plots (not shown). As the spacecraft exits the plasmasheet boundary layer at around 05:10:30 (Panel F), we see the same two beams, but now with a **ExB** velocity double that in the lobe, This middle distribution does show some v_{perp2}, but it is not clear whether this is a time aliasing as the fields change direction during the four-second measurement of the distribution function. The distribution function measured deepest in the plasmasheet (Panel E, at 05:09:58), shows the highest parallel and **ExB** drift speeds, and no significant v_{perp2}. For additional information on this event see *Nakamura et al.* (this volume).

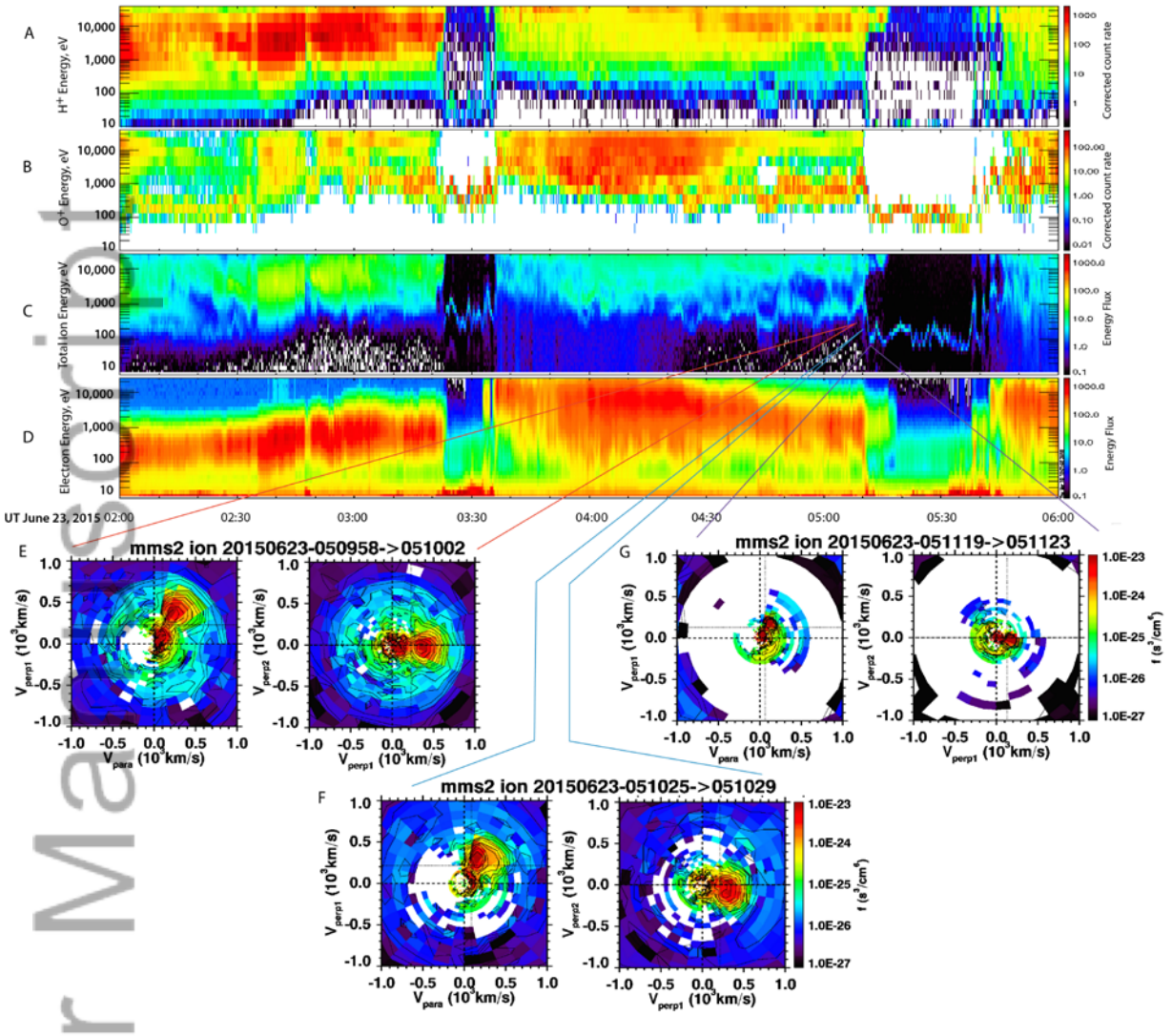

Figure 3. HPCA (MMS1) and FPI (MMS2) measurements in the magnetotail from 0200 to 0600 of June 23. Energy spectrograms of the HPCA H^+ (Panel A) and O^+ (Panel B) corrected counts are shown in the top two panels with Panel B showing an O^+ beam from the ionosphere merging into the plasma sheet at each lobe/plasmasheet transition. FPI ion and electron spectrograms of differential energy flux are shown respectively in Panels C and D. The bottom three panels (E, F and G) show three pairs of FPI distribution functions as the spacecraft exited the plasmasheet to the lobe. The left of each pair shows $v_{parallel}$ and v_{perp1} (along **E**x**B**) components of the particle distribution functions, and the right of each pair shows the two perpendicular velocities, v_{perp1} and v_{perp2}.

At the same time, the magnetic fields observed at MMS in the tail and by VAP closer to the Earth showed dramatic dipolarizations as the magnetotail responded to the Northward turnings of the IMF (Figure 4). At MMS-1 (top), the measured Bx went from -90 to -20nT, and Bz

increased from near zero to 30nT. The transitions from MMS from the plasmasheet to the lobe resulted primarily because of the thinning and expansion of the plasmasheet and partially because of the flapping of the magnetotail current sheet up and down.

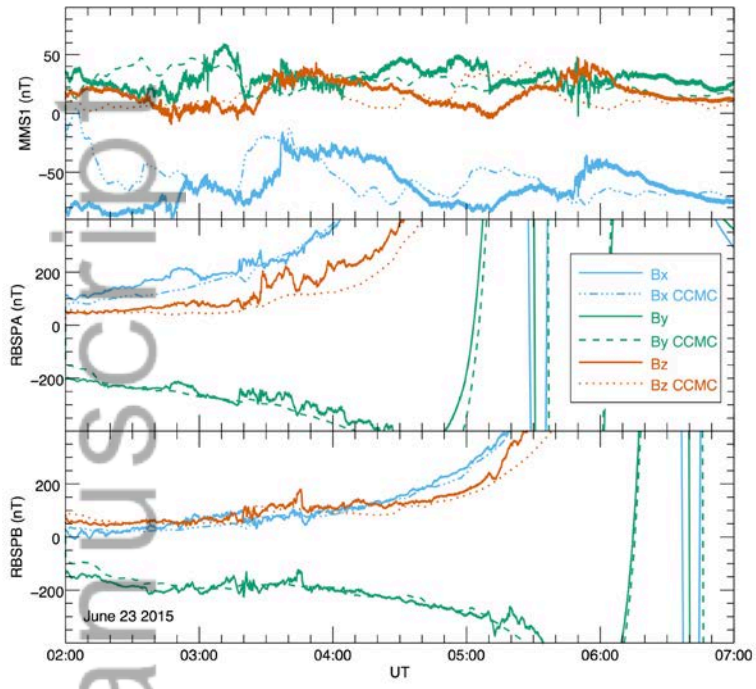

Figure 4. Tail magnetic fields observed by MMS1 (top) and Van Allen Probes A (middle) and B (bottom) (solid lines) and modeled (dashed lines) using a high-resolution run of BATS-R-US from the CCMC.

4 Modeling Results

To put these observations into context we ran the BATS-R-US model [*Powell et al.*, 1999; *Tóth et al.*, 2005, 2012] with RCM in highest resolution available from the Coordinated Community Modeling Center (CCMC) (5 minute cadence and 1/8 RE at the inner boundary), using the measured propagated solar wind and IMF from OMNIdata. The model showed many tail reconnection events in the time frame of 00:00 UT on June 22 to 24:00 UT on June 23. Movies showing various cuts of the model for this event, including a cut that dynamically followed the MMS trajectory, can be found in the Supplemental material and at http://mms.rice.edu/June22. The model did especially well at capturing the several stretching and rapid dipolarizations observed in the 2-6 UT June 23 time frame (Figure 4, dashed). The first dipolarization in the model was between 3:15 and 3:20 (Figure 5A) and was observed at MMS at 3:16 [*Nakamura et al.*, this volume]. The second dipolarization in the model occurred between 04:55 and 05:00, seen at MMS at ~5:10 (See the movie *62223MMScut.mp4* in the supporting information). The

magnitude of the field changes predicted along the MMS path were quantitatively accurate, but with some variances in timing, reaching peak values somewhat earlier than measured. The model suggests that at the times of the dipolarizations, an x-line is just downstream of MMS, which is very near the separatrix (Figure 5A). Since the tail was so stretched, a modest flapping of the tail affects the location of MMS relative to the model. The dipolarization signatures observed at VAP RBSP-A (middle panel of Figure 4) were accurate in location but low in amplitude. The dipolarization signatures observed at RBSP-B (lower panel of Figure 4) showed good agreement both in magnitude and location. Thus we argue that the O^+ ions seen flowing downstream in the lobe near the edge of the plasmasheet may be captured by the reconnection process and become the energetic O^+ seen in the plasmasheet.

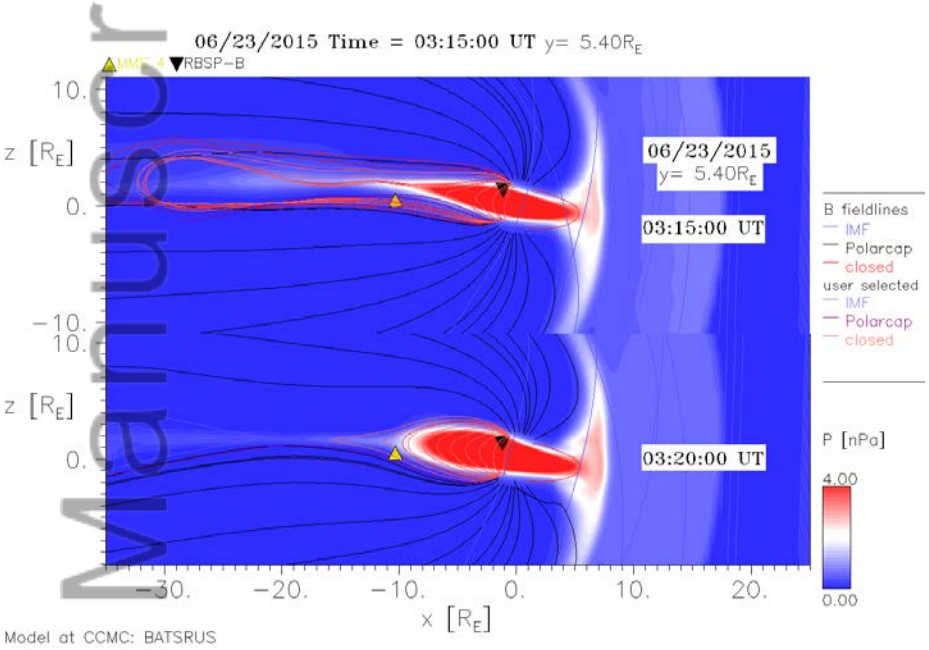

Figure 5A. Two frames from a movie of the CCMC run, showing MMS 1 spacecraft located very near the separatrix of an x-line in the magnetotail. The dipolarization in the model is well observed between the stretched configuration of 03:15 and the more dipolar configuration of 03:20. The full movie including similar frames for the 05:00 dipolarization is in the supplementary materials and is available at http://mms.rice.edu/June22/.

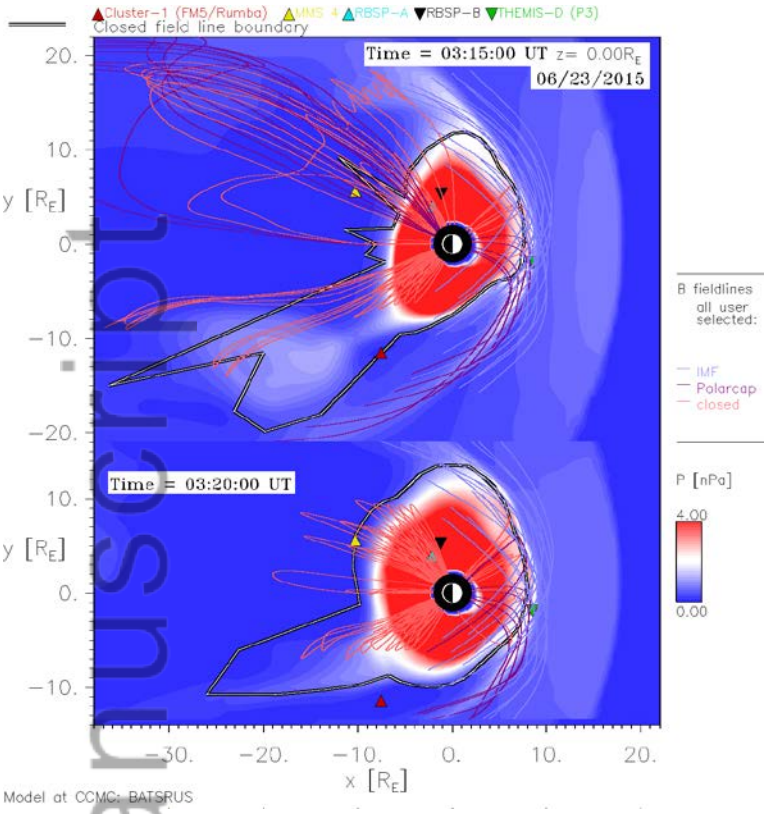

Figure 5B. Similar to 5a, but showing the equatorial plane locations of the various magnetospheric spacecraft (MMS, VAP-A and B, Themis, Cluster) at the time of the dipolarization. The field lines in both times were started at the same locations on the equatorial plane. Note how less stretched each field line is after the dipolarization. A movie of this view is provided in the supplementary materials and on our website http://mms.rice.edu/June22

When mapped to the ionosphere, the model showed extremely large field-aligned currents (FAC). As compared to the FAC's inferred from the AMPERE data [e.g. *Coxon et al.*, 2014], which reached an integrated value of nearly 25 MA, the predicted magnitudes were 20-50% smaller than that observed, although the timing structure was quite accurate (Figure 2E-F).

5 Polar Cap Convection Patterns

Because of the large magnetic field strengths (~40 nT) and the large and variable IMF y-component, the model-predicted ionospheric convection varied from normal two-cell convection patterns during times of large negative Bz (Figure 6A), to a four-cell during high positive IMF Bz intervals (Figure 6B) to a single convection cell rotating in opposite directions (clockwise in the North, counter-clockwise in the South) in the two hemispheres after a long interval of strong +By (Figure 6C). A true single cell convection pattern is very rare: in this case the single cell was only predicted (and observed) in the North. A movie of the modeled convection patterns

62223_ionosphere.mp4 is part of the supplemental information and posted at http://mms.rice.edu/June22.

A comparison with DMSP plasma flow data from the same intervals confirms the basic features of the convection, but interesting differences are observed. For example, in the southward IMF case (6A), the polar cap is larger in the data than in the model by about 5 degrees. The sunward flow channel in the data during northward IMF (6B) is much narrower than in the model, which predicts a very large area of sunward flow in the polar cap. The model also missed the strong low-latitude sunward flows on the dusk side. The DMSP flow data confirm presence of a single-cell convection pattern in the North (Figure 6C, bottom right), with just a hint of a viscous cell at 7MLT, 75 ILAT. The cross-polar cap potential drops estimated from the model and from the flow data are comparable. Both the model and the data show the center of the cell just duskward of the magnetic pole. The lobe cell convection is more common in times of high sunward dipole tilt [*Crooker, 1992*], and this event which occurred on June 22- 23, had maximum sunward tilt in the North.

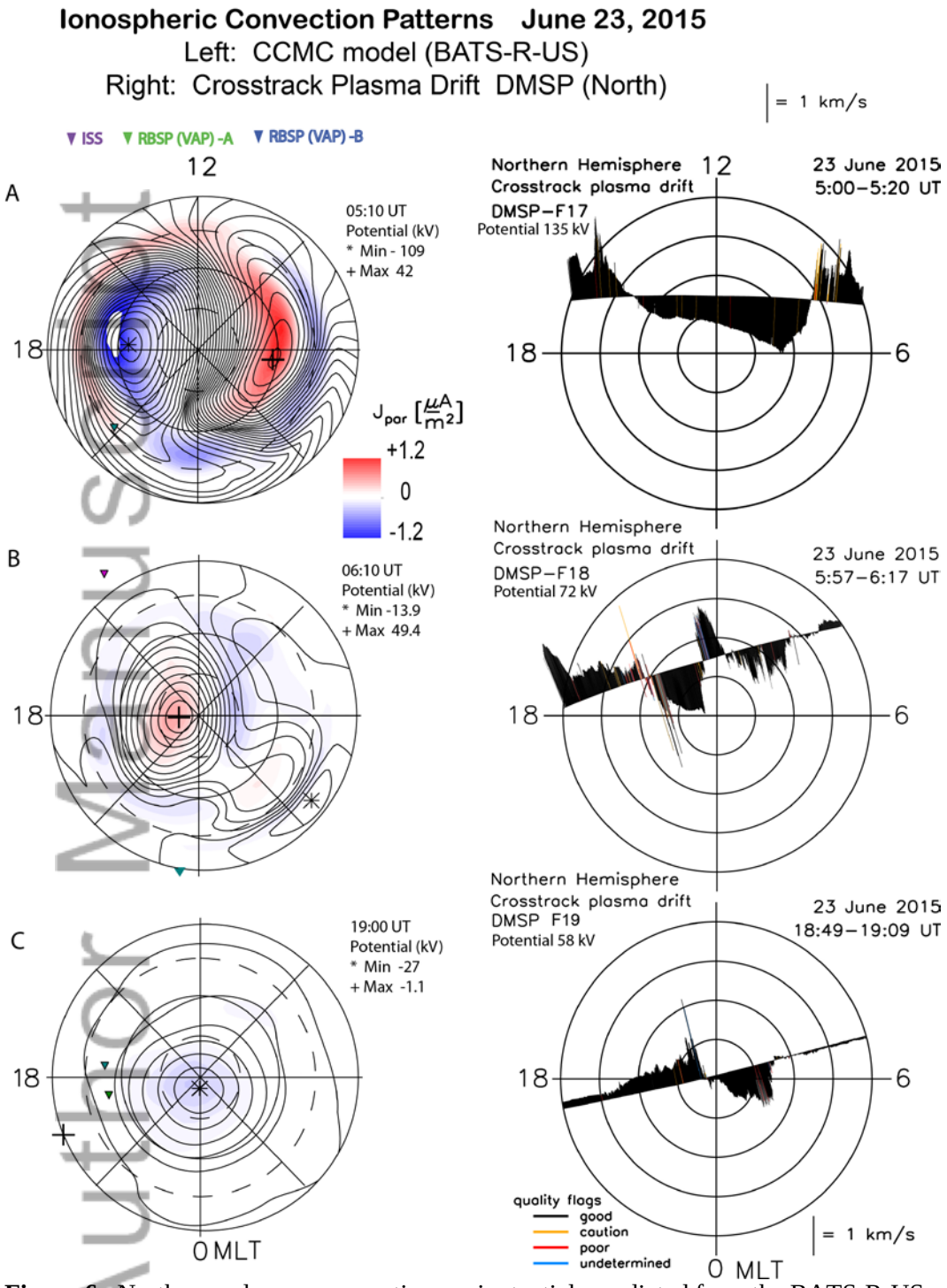

Figure 6. Northern polar cap convection equipotentials predicted from the BATS-R-US run (left image in each row). Colored areas are the field-aligned current densities, and equipotential lines are 4kV apart

in each plot. The movie is available at http://mms.rice.edu/June22. Right side: measured crosstrack plasma drifts from DMSP at the same time as the predicted potentials. Panel A is a normal two-cell convection pattern during southward IMF; Panel B is a four-cell pattern with reversed flow in the central polar cap during strong northward IMF; Panel C is a single-cell clockwise convection observed during strong positive Y-component of the IMF.

6 Conclusions

This event represents the first major storm of the new Heliospheric Flotilla era. With well-instrumented spacecraft strategically placed in the magnetosphere, and new computational models, our understanding of magnetospheric dynamics, especially its response during dramatic events such as the one presented in this paper, is taking a leap forward. Despite this being an anomalously intense event with large magnetic fields, the BATS-R-US model did an admirable job of reproducing the amount of field change during the dipolarizations, estimating the polar cap convection and currents, and the approximate location of MMS near the separatrix during a very dynamic magnetotail sequence.

Acknowledgements

The authors thank the MMS team for an amazing suite of instruments, and for making high resolution data available even during the commissioning phase. This work was carried out using the SWMF/BATS-R-US tools developed at The University of Michigan's Center for Space Environment Modeling (CSEM) and made available through the NASA Community Coordinated Modeling Center (CCMC). We particularly thank M. Kuznetsova for her help in optimizing the inputs. We thank Craig Kletzing for VAP magnetometer data, and the ACE team for plasma and IMF data through CDAWeb. This study was partially supported by the NASA MMS mission under Contract 599790Q from SWRI to Rice University. It was also partially supported by NASA under grant NNX14AN55G to Rice University and WBS 943396.05.03.02.10.02 to Marshall Space Flight Center. The DMSP analysis was funded by NSF under grant AGS-1259508. All MMS data are now freely available to the community. Animations from the modeling runs are posted at: http://mms.rice.edu/June22. The CCMC run is archived at: http://ccmc.gsfc.nasa.gov/results/viewrun.php?domain=GM&runnumber=Stanislav_Sazykin_111315_1.

References

Bala, R. and P. H. Reiff (2012), Improvements in short-termf of geomagnetic Activity, *Space Weather, 10,* doi:10.1029/2012SW000779.

Bala, R., and P. H. Reiff (2014), Validating the Rice neural network and the Wing Kp realtime models, *Space Weather*, *12,* doi:10.1002/2014SW001075.

Burch, J. L., T. E. Moore, R. B. Torbert and B. L. Giles (2015), Magnetospheric Multiscale overview and science objectives, *Space Sci. Rev.*, doi:10.1007/s11214-015-0164-9.

Coxon, J. C. S. E. Milan, L. B. N. Clausen, B. J. Anderson, H Korth (2014), The magnitudes of the regions 1 and 2 Birkeland currents observed by AMPERE and their role in solar wind-magnetosphere-ionosphere coupling, *J. Geophys. Res,* doi:10.1002/2014JA020138.

Crooker, N. U. (1992), Reverse convection, *J. Geophys. Res.*, **97**, 19,363–19,372, doi:10.1029/92JA01532.

Liao, J., L. M. Kistler, C. G. Mouikis, B. Klecker, I. Dandouras, and J.-C. Zhang (2010), Statistical study of O+ transport from the cusp to the lobes with Cluster CODIF data, *J. Geophys. Res.*, **115**, A00J15, doi:10.1029/2010JA015613.

Liao, J., L. M. Kistler, C. G. Mouikis, B. Klecker, and I. Dandouras (2012), Solar cycle dependence of the cusp O+ access to the near-Earth magnetotail, *J. Geophys. Res.*, **117**, A10220, doi:10.1029/2012JA017819.

Lu, G., P. H. Reiff, T. E. Moore, and R. A. Heelis (2012), Upflowing ionospheric ions in the auroral region, *J. Geophys. Res.*, *97*, p. 16,855-16,863, (1992).

McComas, D. J., S. J. Bame, P. Barker, S. C. Feldman, J. L. Phillips, P. Riley, J. W. Griffee (1998), Solar Wind Electron Proton Alpha Monitor (SWEPAM) for the Advanced Composition Explorer, *Space Sci. Rev.*, *86*, 613, doi:10.1023/A:1005040232597.

Pollock, C. T. Moore, A. Jackes, J. Burch, Ul. Gliese, Y. Saito, T. Omoto, L. Avanov, A. Barrie et al. (2015), Fast Plasma Investigation for Magnetospheric Multiscale, *Space Sci. Rev*., doi:10.1007/s11214-016-0245-4.

Powell, K. G., P.L. Roe, T.J. Linde, T.I. Gombosi, and D.L. De Zeeuw (1999), A Solution-Adaptive Upwind Scheme for Ideal Magnetohydrodynamics, *J. Computational Phys., 154*, 284-309.

Reiff, P. H., and J. L. Burch (1985), By-Dependent plasma flow and Birkeland currents in the dayside magnetosphere: 2. A Global Model for Southward and Northward IMF, *J. Geophys. Res.*, *90*, pp. 1595-1609.

Russell, C. T., B. J. Anderson, W. Baumjohann, K. R. Bromund, D. Dearborn, D. Fischer, G. Le, H. K. Leinweber, D. Leneman et al. (2015), *Space Sci. Rev*., doi: 10.1007/s11214-014-0057-3.

Smith, C. W., J. L'Heureux, N. F. Ness, M. H. Acuña, L. F. Burlaga, and J. Scheifele (1998), The ACE Magnetic Fields Experiment, *Space Science Reviews*, *86*, 613, doi:10.1023/A:1005092216668.

Tóth, G., I. V. Sokolov, T. I. Gombosi, D. R. Chesney, C. R. Clauer, D. L. De Zeeuw, K. C. Hansen, K. J. Kane, W. B. Manchester, R. C. Oehmke, K. G. Powell, A. J. Ridley, I. I. Roussev, Q. F. Stout, O. Volberg, R. A. Wolf, S. Sazykin, A. Chan, and B. Yu (2005), Space Weather Modeling Framework: A new tool for the space science community, *J. Geophys. Res*., 110, A12226, 2005. doi: 10.1029/2005JA011126.

Tóth, G., B. van der Holst, I.V. Sokolov, D.L. De Zeeuw, T.I. Gombosi, F. Fang, W.B. Manchester, X. Meng, D. Najib, K G. Powell, Q. F. Stout, A. Glocer, Y.-J. Ma, M. Opher (2012), Adaptive Numerical Algorithms in Space Weather Modeling, *J. Computational Phys*., 231, 870-903, doi: 10.1016/j.jcp.2011.02.006.

Young, D. T., J. L. Burch, R. G. Gomez, A. De Los Santos, G. P. Miller et al. (2015), Hot Plasma Composition Analyzer for the Magnetospheric Multiscale Mission, *Space Sci. Rev*., doi: 10.1007/s11214-014-0119-6.

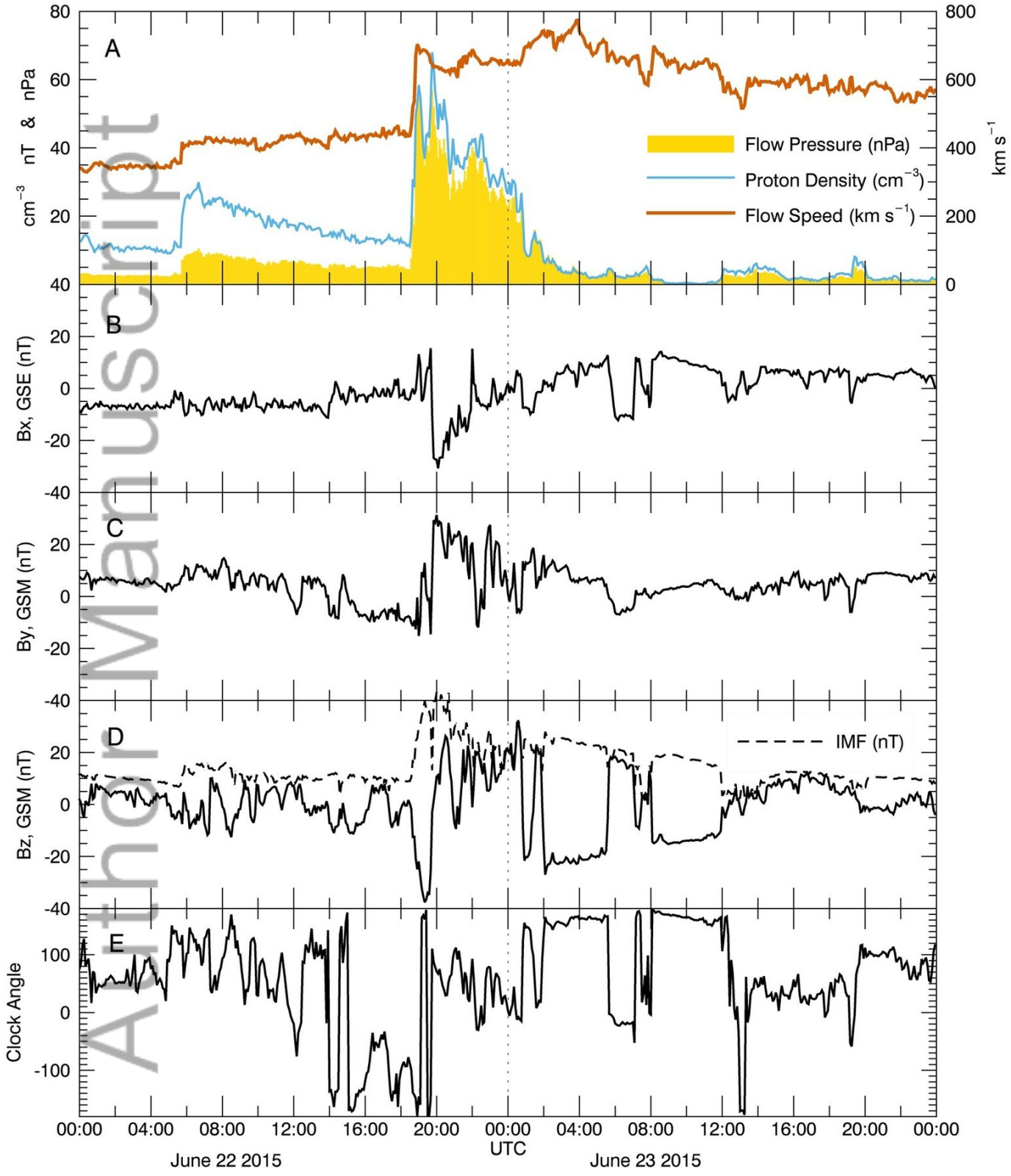

2016GL069154-f01-z-.jpg

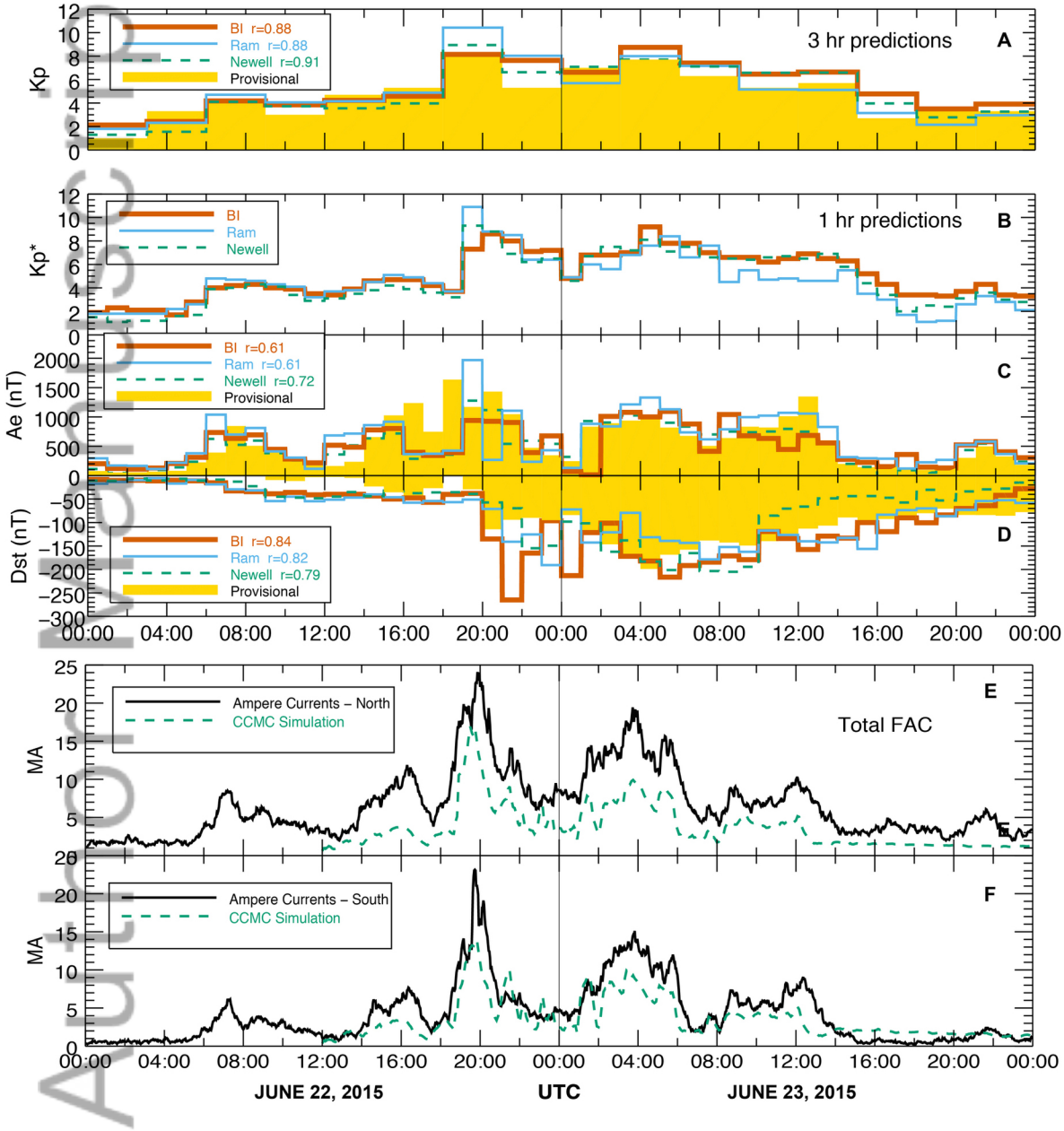

2016GL069154-f02-z-.jpg

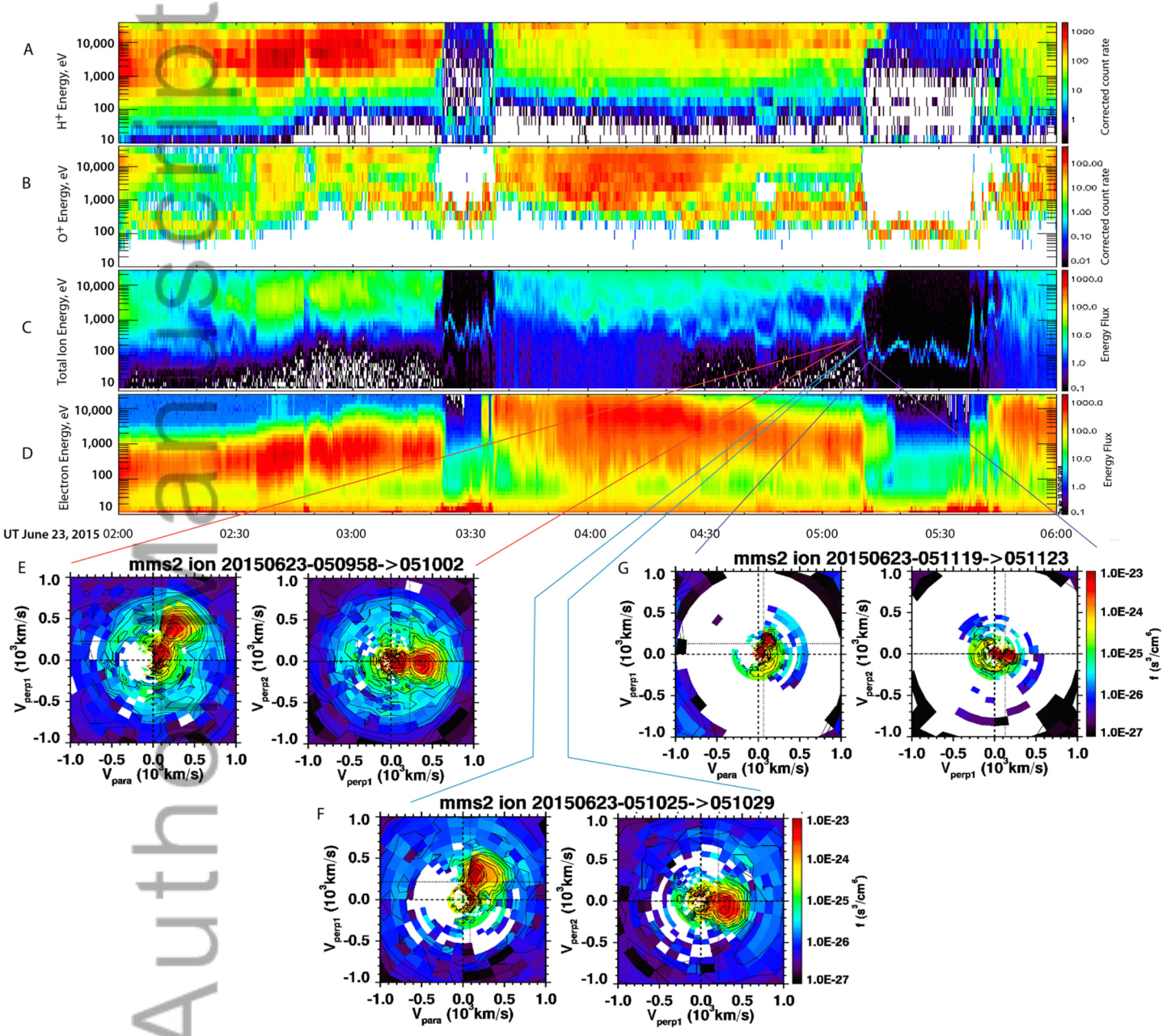

2016GL069154-f03-z-.jpg

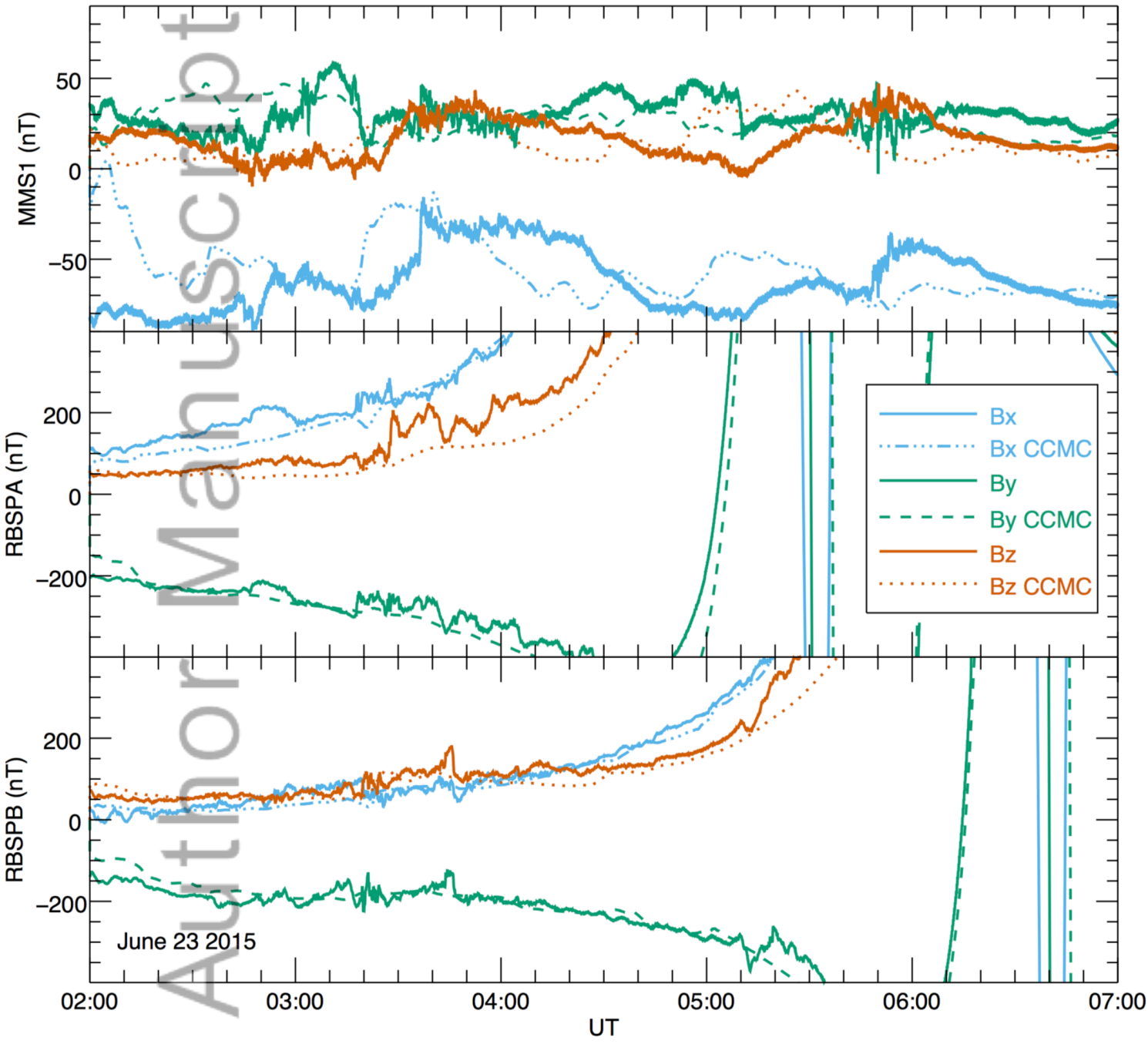

2016GL069154-f04-z-.png

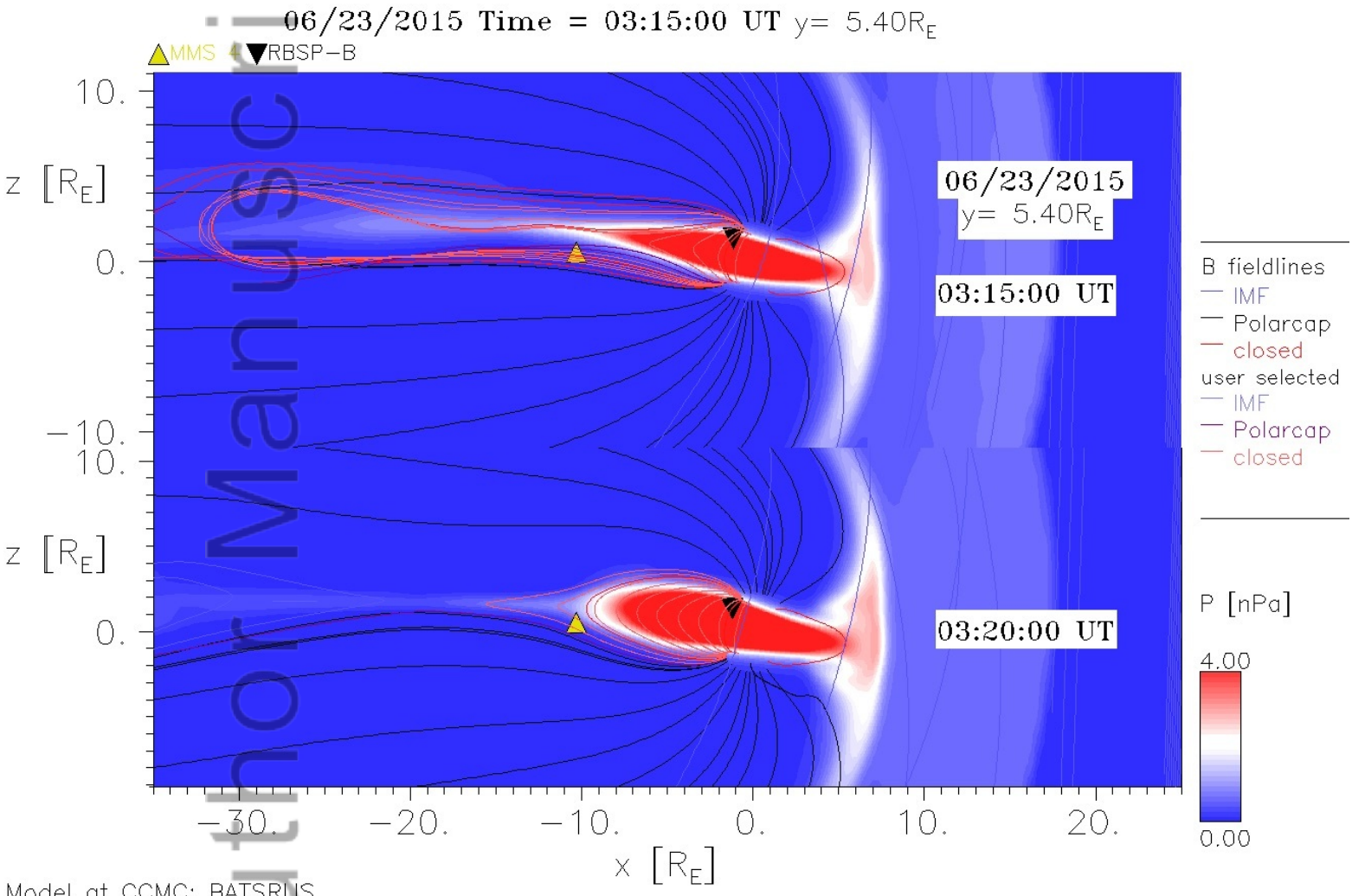

2016GL069154-f05-z-.jpg

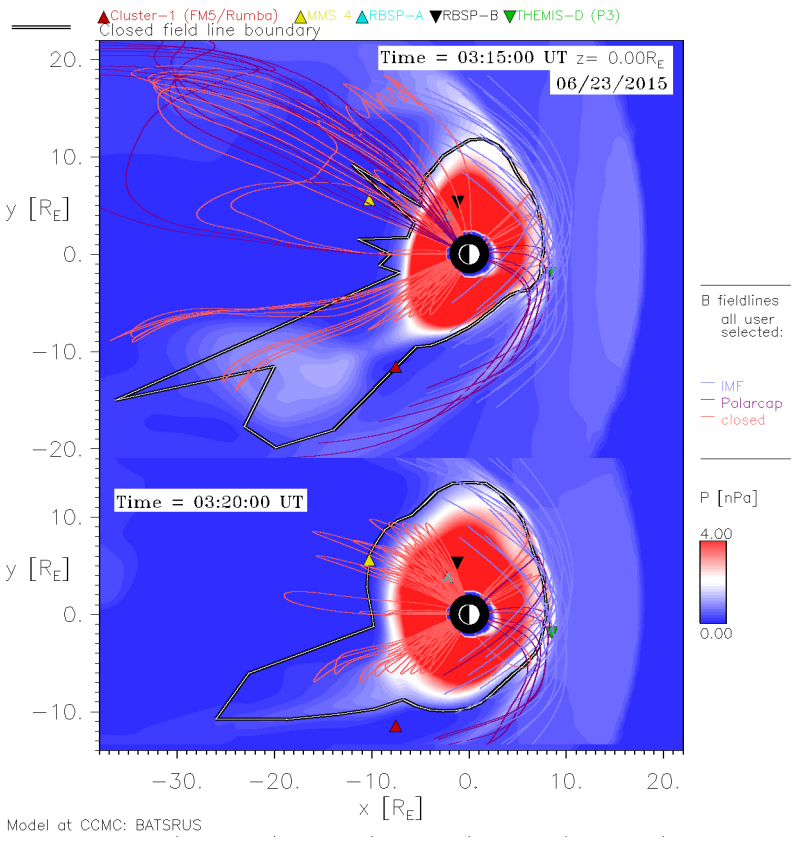

2016GL069154-f06-z-.jpg

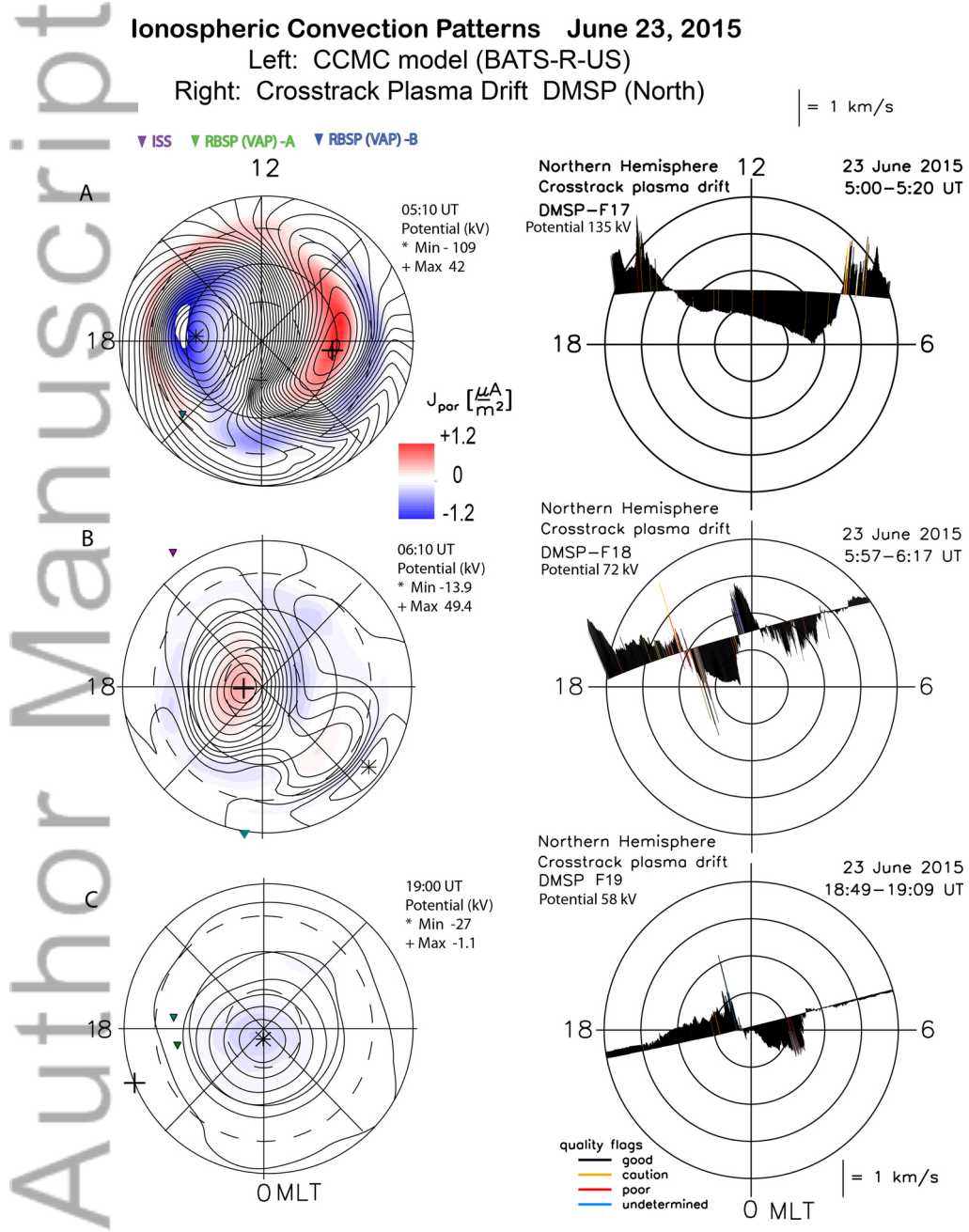

2016GL069154-f07-z-.jpg